ARTICLE

A Light-controlled, Solvent-induced Spin-State Switching in a 3D Hexagonal Heterobimetallic Network

Received 00th January 20xx,
Accepted 00th January 20xx

DOI: 10.1039/x0xx00000x

Krishna Kaushik,[a] Suprabha Pradhan, [a] Sakshi Mehta, [a] Sujit Kamilya, [a] Rodrigue Lescouëzec,[b] Pradip Kumar Mondal,[c] Mathieu Rouzières,[d] Jiri Pechousek,[e] Yanling Li [b] and Abhishake Mondal*[a]

A cyanide bridged {4d-3d} heterobimetallic assembly of Mo^{V}-Fe^{II} with formula $\{[Mo^{V}(CN)_8][Fe^{II}(v\text{-}im)_4]_2\cdot BF_4\}_n$ 2DMF·H_2O (1·2DMF·H_2O) was achieved by the self-assembly of $[Mo(CN)_8]^{3-}$ and iron(II) with monodentate nitrogen donor ligand v-im (v-im = 1-Vinylimidazol). The complex was fully characterized by single-crystal X-ray diffraction analyses, spectroscopic and (photo)magnetic studies. Single crystal X-ray analyses revealed that the complex exhibits a three-dimensional (3D) hexagonal network structure of molybdenum(V) and iron(II) centers bridged by the cyanide ligands. The partially desolvated form 1·2DMF exhibit thermo-induced spin crossover (SCO) between LS Fe(II) and HS Fe(II) center over a wide range of temperature and light-controlled spin-state switching phenomenon at low temperature under light irradiation with T_{LIESST} = 70 K whereas the fully solvated complex 1·2DMF·H_2O remains in the HS state. This complex represents the first 3D coordination complex consists of iron(II) and $[Mo^{V}(CN)_8]^{3-}$ units exhibiting reversible and complete SCO phenomenon and photo-magnetic effect.

Introduction

The proficiency of molecule based magnetic materials in controlling their functionalities with external stimuli is an extremely intriguing and appealing trait. A remarkable contribution is attributed to the field of bistable magnetic materials by the spin crossover (SCO) systems where bistability occurs as a result of switching between low-spin (LS) and high-spin (HS) states of d^4–d^7 transition-metal complexes.[1-4] Extensive studies have been carried out over the years with these SCO systems due to their responses towards various external stimuli such as temperature, pressure, light, pH, electric and magnetic fields to change their physical properties as well as functionalities.[5-7] Hence, such materials are the great prerequisites for the design of several multifunctional materials including data storage devices, sensors and switches.[6, 8-11]

Among all the categories of spin-crossover systems, Fe(II) complexes having FeN_6 environment emerged as a prominent candidate of extensive research due to their remarkable diversity in terms of spin transition characteristics.[3, 12-15] The distinction between the paramagnetic HS $[(t_{2g})^4(e_g)^2]$ (S = 2) and diamagnetic LS state $[(t_{2g})^6(e_g)^0]$ (S = 0) of these systems can easily be studied by magnetic, optical and structural changes that occurred during the spin-state switching.[4, 16, 17] However, the SCO solely depends on the nature of the ligands, solvent molecules, structural matrix, counter cations / anions, guest molecules *etc*.[18, 19] Recently, using octacyanometallate building blocks $[M^{IV/V}(CN)_8]^{4-/3-}$ (M = Mo, W, Nb, Re) and SCO active Fe(II) units, we have explored the multifunctional properties of SCO materials that can point towards the development of advanced bistable materials with improved functionalities.[20-22] Our recent studies revealed that, bimetallic assemblies of extended coordination networks based on octacyanometallate building blocks are good candidates as they can offer eight coordination sites coming from eight cyanide ligands and can have various structural topologies ranging from one dimensional to three-dimensional networks.[20, 23-25] Most importantly, the topology of structures formed by these complexes are extremely variant and shows important physical as well as chemical properties.[23, 26] It is worth noting that very few Fe(II) SCO systems connecting with $[Mo^{IV/V}(CN)_8]^{n-}$ building blocks have been reported so far and among them 3D network exhibiting complete SCO property is very rare in the literature.[21, 27-30] In this regard to design the multifunctional magnetic material we have synthesized a novel 3D cyanide-bridged hexagonal coordination network based on octacyanometallate building block which exhibits solvent-

[a] *Solid State and Structural Chemistry Unit, Indian Institute of Science, Sir C V Raman Road, Bangalore 560012, India. Email: mondal@iisc.ac.in, http://m2sscuiisc.in.*
[b] *Institut Parisien de Chimie Moléculaire, CNRS UMR 8232, Sorbonne Université, 4 place Jussieu F-75252 Paris, cedex 5, France.*
[c] *Elettra - Sincrotrone Trieste S.C. p. A., S.S. 14, Km 163.5 in Area Science Park, Basovizza 34149, Italy.*
[d] *University of Bordeaux, CNRS, Centre de Recherche Paul Pascal, CRPP, UMR 5031, 33600 Pessac, France*
[e] *Department of Experimental Physics, Palacký University Olomouc, 17. listopadu 1192/12, 771 46 Olomouc, Czech Republic*
Electronic Supplementary Information (ESI) available: Additional information about selected experiments, IR spectra, UV spectra, magnetic data and crystallographic tables.

triggered reversible spin-state switching and Light-Induced Excited Spin State Trapping (LIESST) effect at low temperature. Applying complex as ligand strategy, herein we used octacyanometallate $(HNBu_3)_3[Mo^V(CN)_8]$ building block to prepare a 3D hexagonal coordination network of formula $\{[Mo^V(CN)_8][Fe^{II}(v\text{-}im)_4]_2\cdot BF_4\}_n$ 2DMF·H_2O (**1**·2DMF·H_2O) [v-im = 1-Vinlyimidazole] and studied the structural, spectroscopic, (photo)magnetic, and electrochemical properties.

Results and discussion

Synthesis and characterization

The reaction of $[HNBu_3]_3[Mo(CN)_8]$ with a mixture of $Fe(BF_4)_2.6H_2O$ and v-im in DMF resulted in a green solution. Slow evaporation of the reaction mixture afforded analytically pure yellow plates shape crystals of 1·2DMF·H_2O (Figure S1) in good yield (details in supporting information). PXRD and elemental analysis were performed to check the purity of 1·2DMF·H_2O in bulk (Figure S2). 1·2DMF·H_2O experiences a weight loss between 300 and 313 K (WL: 1.5%) and converts to partially desolvated form of 1·2DMF after losing one water molecule from the crystal structure, after which the complex is stable up to 430 K, confirmed by TGA analysis (Figure S3). The minor deviation in the experimental PXRD data is seen due to the temperature difference between experimental and simulated data and the partial loss of interstitial solvent molecules during the sample preparation for the PXRD measurement at room temperature.

Crystal Structure Analyses

Single-crystal X-ray diffraction of 1·2DMF·H_2O was performed at 120 and 240 K where it crystallizes in a monoclinic space group *C*2/c forming a 3D hexagonal coordination network (Table S1) connecting the molybdenum and iron centers via cyanide bridge. The asymmetric unit is made up of two crystallographically independent Fe(II) centers on a glide plane and one Mo(V) center on a 2-fold axis, with each contributing half to the unit cell along with one BF_4^- counter anion and two DMF and one water molecule. The coordination geometry of $[Mo^V(CN)_8]^{3-}$ ion is best described as a distorted square antiprism (continuous shape measures (CShM)[31] program, Table S8-S9) with MoC_8 surrounding from four terminal and four carbon donor atoms from four bridging cyanide ligands. The Fe(II) ions are six-coordinate and adopt pseudo-octahedral geometry both in 120 and 240 K confirmed by CShM analysis (Table S8-S9). The coordination environment around Fe1 and Fe2 centers are satisfied with four imidazolyl nitrogen atoms coming from the vinyl imidazole ligand and two nitrogen atom of bridging cyanide group from $[Mo(CN)_8]^{3-}$. Among the four bridging cyanides of $[Mo(CN)_8]^{3-}$ unit, two of them are bridged with two Fe2 centers along the ac direction and the other two cyanides are bridged to Fe1 along the b direction resulting a 3D hexagonal network (Figure 1 & S4). This alternate cyanide-bridged Mo and Fe 3D network contains 12 membered $\{Mo_6Fe_6\}_n$ hexagonal rings. The water and DMF molecules occupy the pore inside the crystal structure which has a length of 24.880 Å and width of 14.568 Å. There are several H-bonding interactions present in the crystal structure between the solvent molecules (DMF and H_2O) and nitrogen atoms of free cyanide from $[Mo(CN)_8]^{3-}$ unit (Figure S6, left).

The Mo-C bond distances at 120 K in 1·2DMF·H_2O lie in the range of 2.144(3) - 2.158(3) Å for bridging cyanides and for the non-bridging cyanide the value ranges from 2.161(4) – 2.167(3) Å which is typical for Mo(V) state (Table S2).[21] The Fe1-N bond lengths vary from 2.152(3) to 2.174(3) Å which is very similar to those of Fe2-N bond lengths ranging between 2.119(3) – 2.162(3) Å. This suggests that both Fe1 and Fe2 centers are present in a high-spin Fe(II) state at 120 K.[19, 32, 33] At 240 K, the average Mo-C bond distance is observed to be 2.161 Å whereas the average Fe1-N and Fe2-N bond distances are found to be 2.167 and 2.175 Å respectively indicating the presence of Fe(II) HS state (Table S3) at this temperature. After that we have measured the single crystal XRD structure using synchrotron beamline where we introduced the crystal directly at 350 K and rapidly cooling it down to 270 K in order to get the structure of the partially desolvated complex 1·2DMF as suggested by the TGA analysis (*vide supra*). Complex 1·2DMF also crystalizes in monoclinic space group *C*2/c with Mo center adopting distorted square antiprism geometry and Fe centers adopting distorted octahedral geometry (Table S1 & S13). Similar values of Mo-C, Fe1-N and Fe2-N bond distances (avg. Mo-C=2.172; avg. Fe1-N=2.172; avg. Fe1-N=2.161) are observed for the partially desolvated complex (1·2DMF) at 270 K indicating the presence of Fe(II) HS and Mo(V) states at that temperature (Table S4).

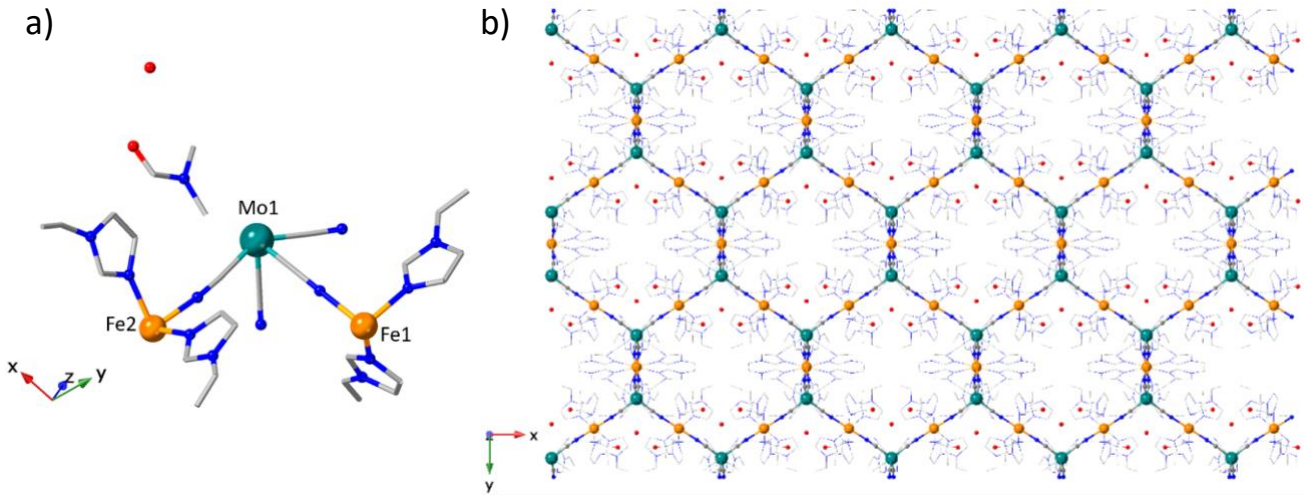

ARTICLE

Fig. 1 a) Perspective view of the asymmetric unit of complex 1·2DMF·H_2O, b) View along the c-direction showing honeycomb like 3D structure formed by 1·2DMF·H_2O. Hydrogen atoms are eliminated for clarity. Fe(II): orange; Mo(V): cyan; C: grey; N: blue; O: red.

The cyanide bridges on the Fe1 and Fe2 are slightly deviated from linearity [Fe1−N9−C21 = 175.1 (3) (120 K), Fe1−N1−C1 = 175.3 (3) (240 K) and Fe2−N11−C22 = 173.2 (120 K), Fe2−N2−C2 = 174.4 (4) (240 K)] for complex 1·2DMF·H_2O (Table S5-S6).

For 1·2DMF the cyanide bridges from Fe sides are also slightly deviated from linearity with values Fe1−N12−C20 = 176.3 (7) and Fe2−N3−C22 = 172.8 (7) (Table S7). All the Mo−C≡N bond angles are nearly linear ranging from 176.04° to 178.83° for both 1·2DMF·H_2O and 1·2DMF. The octahedral distortion parameters ($\sum$, Θ and ζ) and CShM factor calculated from the crystal structure at 120 and 240 K for 1·2DMF·H_2O and at 270 K for 1·2DMF also suggests the presence of Fe(II) HS state for Fe1 and Fe2 in 1·2DMF·H_2O and 1·2DMF (Tables S11- S13).[13, 19, 34, 35]

For 1·2DMF the DMF molecules occupy the pore inside the crystal structure (Figure S5). The pore size is comparable to that of 1·2DMF.H_2O with length of 24.903 Å and width of 14.722 Å. The asymmetric unit has few H-bonding interactions between the DMF molecules, nitrogen atoms of free cyanide from $[Mo(CN)_8]^{3-}$ unit and carbon atoms of v-im ligands. (Figure S6, right).

Spectroscopic studies

The UV-Vis-NIR studies were carried out in the solid state at room temperature to determine the electronic states of 1·2DMF·H_2O (Figure S7). The electronic spectrum shows one sharp band centered at 320 nm ascribed to the ligand-to-metal charge transfer (LMCT) transition coming from the $[Mo(CN)_8]^{3-}$ unit.[21] There is also a very broad charge transfer band present in the range of 600-2000 nm, which can be ascribed to the metal-to-metal charge transfer (MMCT) transition coming from the $Fe^{II} \rightarrow Mo^{V}$ unit. The solution state UV-Vis measurement was unable to perform due to the insolubility of this complex in any conventional organic solvents.

To determine the temperature dependence of oxidation and spin state of the metal center coordinated with cyanide NC^-, variable temperature FT-IR measurements were carried out for 1·2DMF·H_2O and 1·2DMF·in the temperature range of 300 – 100 K (Figures S8-S11). At 300 K, two sharp absorption bands were observed at 2114 cm^{-1} and 2131 cm^{-1}, which are characteristic of ν (C≡N) stretching vibration coming from the free cyanide of building block and bridging cyanide of Mo^{V}-C≡N-Fe^{II}_{HS}, respectively.[27] Upon cooling the sample from 300 K to 100 K, the position of the free cyanide remains the same whereas the stretching vibration of bridging ν(C≡N) shifts to a lower frequency of 2127 cm^{-1} suggesting the possibility of Mo^{V}–C≡N–Fe^{II}_{LS} moiety. The changes that occurred in the ν (C≡N) stretching vibration upon cooling were also reversible upon heating to 300 K (Fig. S10-S11). This study reveals that there is a thermal dependency of the spin states of the system in the temperature range of 300 – 100 K, which is further confirmed by magnetic measurement (*vide infra*).

Magnetic studies

The temperature dependence of magnetic susceptibility measurements were carried out on a polycrystalline sample of 1·2DMF·H_2O at a magnetic field of 10000 Oe in the temperature range of 2−350 K (Figure 2). At 300 K, the measured χT (χ is the magnetic susceptibility equal to M/H per $MoFe_2$ unit) value is 7.14 $cm^3\ mol^{-1}$ K (Figure 2), which lies in the expected range of χT obtained for two noninteracting HS Fe(II) ions (S = 2, g = 2.2) and one LS Mo(V) ion (S = 1/2, g = 2.0). Upon decreasing the temperature, the χT value remains nearly constant up to 60 K and below this temperature, the χT value decreases rapidly to 1.70 $cm^3\ mol^{-1}$ K at 2 K (Figure 2, blue curve). This is probably due to the combination of magnetic anisotropy coming from the HS Fe(II) centres and weak antiferromagnetic interactions between the HS Fe(II) centers connecting via cyanide bridge. When the sample was further heated up to 350 K, 1·2DMF·H_2O experiences a weight loss and converts to partially desolvated form 1·2DMF after losing one water molecule (confirmed by the TGA analysis, *vide supra*). When the complex 1·2DMF cooled down from 350 K to 2 K, an interesting phenomenon has occurred. The χT value starts decreasing smoothly with a decrease in temperature down to 50 K to a value of 1.72 $cm^3\ mol^{-1}$ K and then remains almost constant down to 20 K. The value at 20 K is slightly higher than expected for two Fe(II) ions in a LS state (S = 0) and one LS Mo(V) ion (S = ½) which indicates that residual HS Fe(II) ions are present at this temperature. Below 20 K, the χT value sharply decreases to a value of 0.641 K $cm^3\ mol^{-1}$ at 2 K. This is probably due to the zero-field splitting and or magnetic anisotropy coming from the residual HS Fe(II) ions. In the heating mode, the χT vs T curve follows the same path as that in the cooling mode, which confirms the reversibility of the SCO phenomenon in 1·2DMF without hysteretic behaviour (Figure S15). The $d(\chi T)/dT$ vs T plot between 30 and 250 K of 1·2DMF displays a broad maximum at around 127 K (Figure S16), representing the $T_{1/2}$ temperature for the SCO system between LS and HS species in 1·2DMF. The best fit of the χT *vs*. T data were obtained from the ideal solution model,[36] (Figure S17) which gives all the important thermodynamic parameters for 1·2DMF as ΔH = 5.18(1) kJ/mol, $T_{1/2}$ = 125(1) K, ΔS = 41.50 J/K/mol. These results fall within the anticipated range for the iron(II) SCO systems.[13] The field dependence of magnetization studies for 1·2DMF·H_2O and 1·2DMF were carried out from 0 to 5 T at 2, 5, 6 K and at 2 K respectively (Figure S13, left and Figure S14). At 2 K and 5 T magnetic field, the magnetization value for 1·2DMF·H_2O is 5.26 μ_B which is lower than the expected value coming from one LS Mo(V) ion (S = ½)

and two HS Fe(II) ions (S = 2). The nonsuperposition of data on a single curve in the M vs H/T plot (Figure S12, right) suggests the low-lying excited states or magnetic anisotropy of the HS Fe(II) centers in 1·2DMF·H_2O.

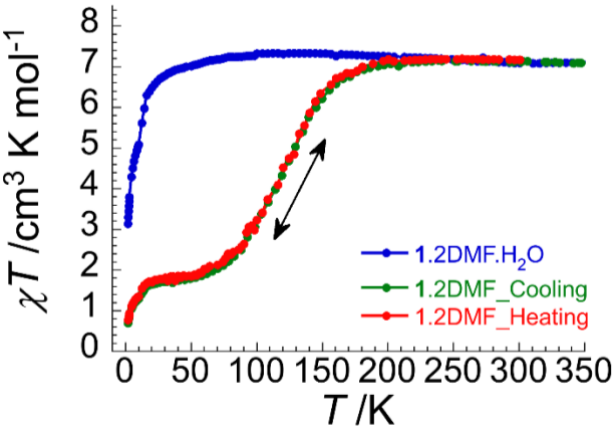

Fig. 2 χT vs T plots of 1·2DMF·H_2O (blue curve) and 1·2DMF (green and red curve) at 10000 Oe external magnetic field.

No in-phase (χ') and out-of-phase (χ'') signal were observed under zero and applied dc field for 1·2DMF·H_2O (Figure S18-S19). At 2 K and 5 T magnetic field, the magnetization value for 1·2DMF is 1.26 μ_B which matched well with one LS Mo(V) ion (S = ½) and LS Fe(II) ions (S = 0) with some contribution from the residual HS Fe(II) centers (Figure S14, red curve).

Optical Studies

The solid-state optical reflectivity studies of the partially desolvated form 1·2DMF was performed in the temperature range of 10–300 K (Figure S20, left) and also under light irradiation at 10 K (Figure 3, left). At 300 K, a broad absorption band centered at around 550 nm was observed which is associated with the MLCT transition coming from HS Fe(II) center (Figure S20, left). Upon decreasing the temperature, the spectra were clearly modified, and a decrease of the absorption band at 550 nm was observed whereas a strong absorption band centered at 700 nm was observed at 10 K, which is due to the change in the spin-state of Fe(II) HS to the Fe(II) LS state (Figure S20, left).

A remarkable change has been evident when analyzing the thermal variation of reflectivity by plotting the absolute reflectivity value at 550 nm against temperature (Figure S20, right). The absolute reflectivity curve shows a gradual decrease upon lowering the temperature from 300 K to 10 K with a minimum at around 60 K. The nature of the curve implies a spin-state switching occurring between HS and LS states at around 120 K, where the magnetic measurements of the powder sample also indicate a comparable $T_{1/2}$ value. A similar behaviour as that of the cooling curve was observed upon heating the sample from 10 to 300 K. The findings of optical studies are in agreement with magnetic studies, confirming the occurrence of reversible spin-crossover phenomenon.

The white light irradiation (180 min, power 0.5 mW/cm^2) of 1·2DMF at 10 K clearly shows a significant increase in the absolute reflectivity spectra (Figure 3, left), even if it is less intense than for the modification with temperature. With a 0.5 mW/cm^2 light power, the photo-excited state was not saturated even after 180 min (Figure S21) light irradiation. Furthermore, light-irradiation experiments were performed using 14 different LEDs ranging from 1050 nm to 365 nm which showed the maximum photoexcitation effect using the 530 nm LED light (Figure S22). After irradiating the sample with 530 nm for 10 min (16 mW/cm^2), an increase in the reflectivity value was observed, indicating the light-induced LS to HS conversion of Fe(II) center in 1·2DMF at 10 K (Figure S23). When the sample was heated keeping the light on, it showed a gradual thermal de-excitation corresponding to the relaxation of the photo-induced metastable Fe(II) HS state into the diamagnetic Fe(II) LS ground state at 70 K (T_{LIESST}) (Figure 3, right).

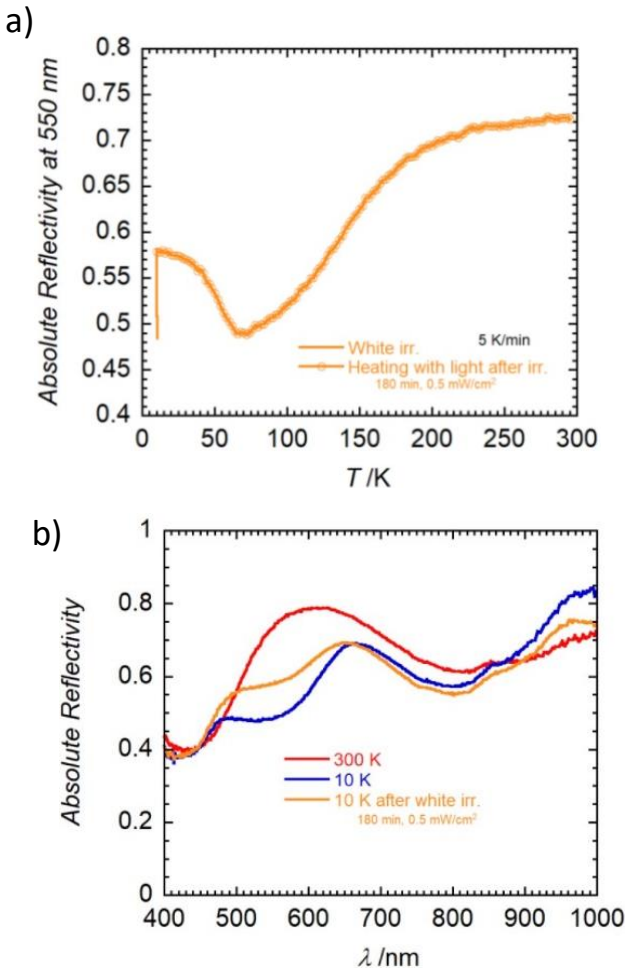

Fig. 3. a) Comparison of the surface reflectivity spectra of 1·2DMF at 300 K (red) and 10 K (blue) in the dark and after 180 min of successive white light (orange) irradiation at 10 K. b) Thermal evolution of reflectivity signal plotted at 550 nm during white light irradiation (0.5 mW/cm^2, at 10 K) and in heating mode in dark (10-300 K, at 5 K/min) for 1·2DM

Mössbauer Studies

To understand fully the spin-state switching phenomenon and the electronic and spin-states of the iron centres present in both complexes 1·2DMF·H_2O and 1·2DMF, ^{57}Fe Mössbauer spectroscopic studies were carried out for both solvated and desolvated sample at 5, 90, 120 and 300 K (Figure 4, Figure S24-25, Table S14). For the fully solvated sample (1·2DMF·H_2O), two quadrupole doublets associated

with parameters typical for HS-Fe^{II} (HS(A): d = 0.94 mm s^{-1}, ΔE_Q = 2.15 mm s^{-1} and HS(B): d = 1.41 mm s^{-1}, ΔE_Q = 2.15 mm s^{-1}) (two quadrupole doublets are observed due to the presence of two unique Fe(II) centers in the asymmetric unit) and one quadrupole doublet associated with LS-Fe^{II} (d = 0.45 mm s^{-1}, ΔE_Q = 0.34 mm s^{-1}) were observed at 5 K with a HS(A)/HS(B)/LS ratio of 44.6/48/7.5 suggesting the presence of small amount of Fe(II) LS this is due to the partial conversion of 1·2DMF·H_2O into 1·2DMF while preparing the sample for Mössbauer experiments. While increasing the temperature to 90 K, a slight increase in the peak intensity of the HS-Fe^{II} (HS(A): δ = 0.90 mm s^{-1}, ΔE_Q = 2.21 mm s^{-1} and HS(B): d = 1.41 mm s^{-1}, ΔE_Q = 2.19 mm s^{-1}) was observed and that of the LS-Fe^{II} (δ = 0.35 mm s^{-1}, ΔE_Q = 0.16 mm s^{-1}) peak intensity decreases with HS(A)/HS(B)/LS ratio of 47.3/47.4/5.2.

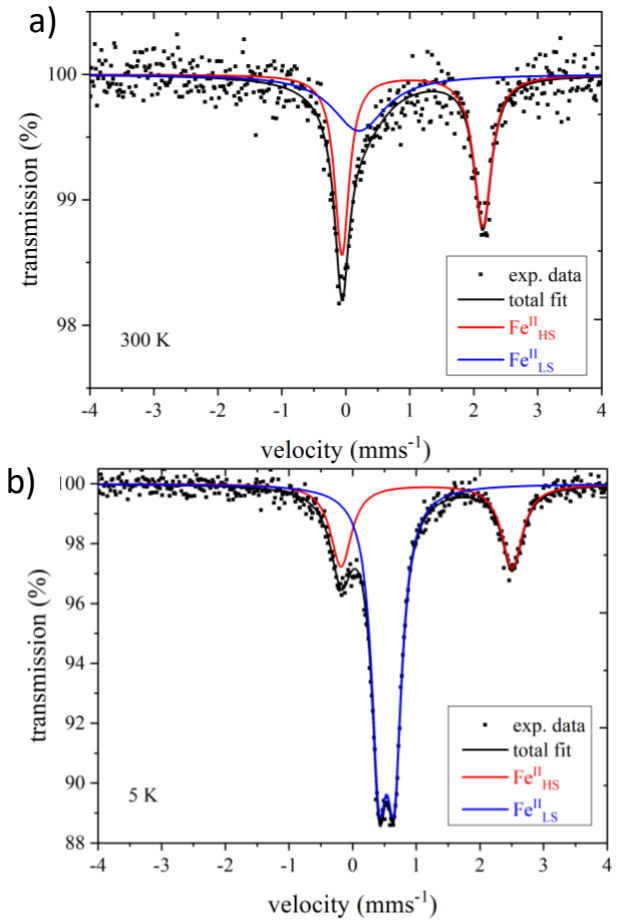

Fig. 4. Mössbauer spectra of 1·2DMF at 5 K (a) and 300 K (b). Blue and red curves represent the quadrupole doublets of the LS-Fe(II) and HS-Fe(II) ions, respectively.

Further increase of temperature to 120 K and 300 K shows the presence of almost 50:50 Fe(II) HS species (HS(A)/HS(B): 49.1/50.9 at 120 K and HS(A)/HS(B): 47.2/52.8 at 300 K) coming from two independent Fe(II) centers with IS and QS parameters δ = 0.90 mm s^{-1}, ΔE_Q = 2.16 mm s^{-1} ; d = 1.40 mm s^{-1}, ΔE_Q = 2.15 mm s^{-1} and δ = 0.89 mm s^{-1}, ΔE_Q = 1.68 mm s^{-1}; d = 1.20 mm s^{-1}, ΔE_Q = 1.67 mm s^{-1} respectively, confirmed the presence of two independent HS Fe(II) centres in 1·2DMF·H_2O. Similarly, the partially desolvated sample (1·2DMF) at 5 K exhibits two quadrupole doublets with d = 1.16 mm s^{-1}, ΔE_Q = 2.69 mm s^{-1} and 0.53 mm s^{-1}, ΔE_Q = 0.24 mm s^{-1} corresponding to HS-Fe^{II} and LS-Fe^{II} respectively suggesting the presence of residual Fe(II) HS at 5 K with HS /LS ratio of 30.5/69.5. At 90 K, a slight increase in the peak intensity of the HS-Fe^{II} (δ = 1.15 mm s^{-1}, ΔE_Q = 2.81 mm s^{-1}) was observed and the LS-Fe^{II} (δ = 0.53 mm s^{-1}, ΔE_Q = 0.24 mm s^{-1}) peak intensity decreases (HS/LS ratio 36.7/63.3). Upon further increasing the temperature to 120 K, the HS-Fe^{II} intensity (δ = 1.13 mm s^{-1}, ΔE_Q = 2.81 mm s^{-1}) increases and LS-Fe^{II} intensity (δ = 1.13 mm s^{-1}, ΔE_Q = 2.81 mm s^{-1}) decreases further with a HS /LS ratio of 57.9/42.1. Finally at 300 K, the amount of HS Fe^{II} ions increases notably (δ = 1.13 mm s^{-1}, ΔE_Q = 2.81 mm s^{-1}) with presence of small amount of residual LS-Fe^{II} ion (δ = 1.13 mm s^{-1}, ΔE_Q = 2.81 mm s^{-1}) with a HS /LS ratio of 63.5/36.5. The relative amounts of $Fe^{II}_{LS}/Fe^{II}_{HS}$ ions derived from the Mössbauer spectroscopic studies, as depicted in Table S14 for 1·2DMF.H_2O and 1·2DMF were in good agreement with the magnetic studies (*vide infra)*.

Gas Adsorption Studies

N_2 adsorption study on the desolvated sample of 1·2DMF was carried out to investigate the porous nature of the complex. The BET adsorption isotherm showed a significant N_2 uptake at 77 K and a type III absorption behaviour (Fig. S 1). The BET surface area and pore volume was found to be 3.7135 m^2g^{-1} and 0.8532 cm^3g^{-1}. The average pore diameter of 41.792 nm indicates the mesoporous nature of the complex 1·2DMF.

Photomagnetic Studies

The photosensitivity of the partially desolvated form 1·2DMF was probed by measuring χT as a function of time while irradiating with 532 and 808 nm laser lights having power in the range 5 - 12 mW/cm^2 at 10 K and 10000 Oe external magnetic dc field. Laser irradiation increased the χT values, with 532 nm light having the most pronounced effect (Fig. S26), causing the χT value to rise over time and eventually reach a near-saturation value of 5.24 cm^3 mol^{-1} K (~73% conversion). The χT value corresponds an incomplete photoconversion of Fe(II)LS state to the Fe(II) HS metastable state at 10 K. The photo-induced metastable state, $(Mo^V_{LS})(Fe^{II}_{HS})_2$ relaxed back to the ground state, $(Mo^V_{LS})(Fe^{II}_{LS})_2$ with a T_{LIESST} of 60 K upon heating (Fig. 5, a). The reverse-LIESST effect was also studied by using 808 nm laser light which converts the photoinduced metastable state to the ground state with 59% photoconversion. The ON/OFF photo-switching cycles for 1.DMF were conducted by measuring the χT as a function of time through multiple cycles of alternating irradiation with 532 nm and 808 nm lasers at 10 K in the presence of a 10000 Oe dc field (Fig. 5, b). Exposure to 532 nm laser light raised the χT value from 1.84 to 5.21 $cm^3mol^{-1}K$, and upon switching off the 532 nm laser, the χT value again jumped to 5.85 $cm^3mol^{-1}K$ due to local heating caused by the laser. Upon irradiating the photoexcited state with 808 nm light, the χT value decreased to 2.84 $cm^3mol^{-1}K$ suggesting the conversion of the metastable state to the ground state. These findings indicate a reversible ON/OFF photo-switching of the Fe(II) center, where the metastable $(Mo^V_{LS})(Fe^{II}_{HS})_2$ state reversibly converts to the ground $(Mo^V_{LS})(Fe^{II}_{LS})_2$ state through spin-state switching via alternating irradiation with 532 nm and 808 nm lights at 10 K.

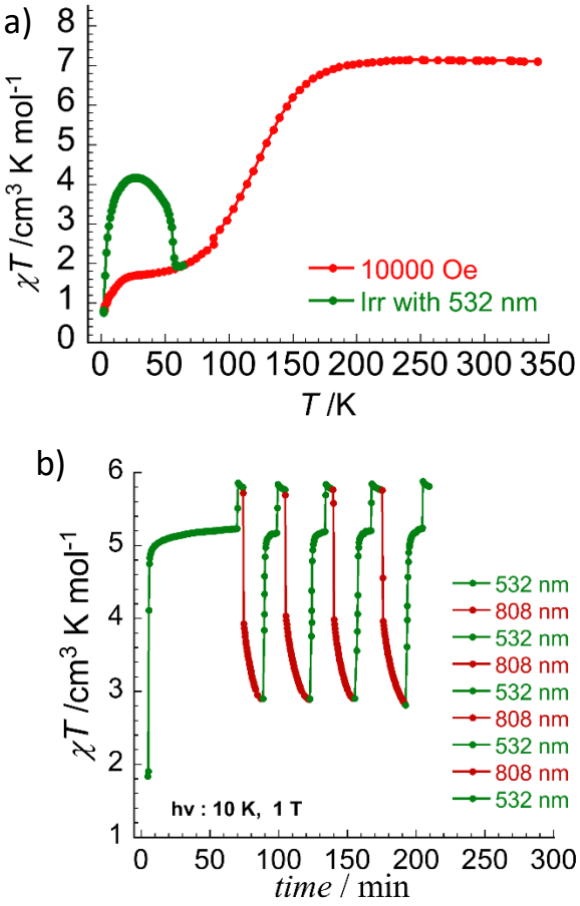

Fig. 5. (a) Temperature dependence of the χT of 1·2DMF after 532 nm light irradiation (green dot) at 10000 Oe. (b) ON-OFF Cycles of χT vs time plot using successive irradiation with 532 and 808 nm at 10 K for 1·2DMF.

Conclusions

In In conclusion, we have successfully synthesized a unique coordination framework based on $[Mo(CN)_8]^{3-}$ building block and Fe^{2+} ions with monodentate N-donor ligand. The crystal structure revealed that 12 membered cyanide bridged $\{Mo_6Fe_6\}$ hexagonal rings are connected in three dimension to form a cyanide-bridged Mo and Fe 3D hexagonal coordination network. X-ray diffraction studies at different temperatures showed the changes in the crystal structure of the complex with respect to temperature. The solvated form (1·2DMF·H_2O) of the 3D network displayed a paramagnetic nature in the χT vs T plot whereas thermo-induced reversible spin-state switching below room temperature was observed for the partially desolvated (1·2DMF) form. The Mössbauer spectroscopic analysis at various temperatures, conducted on both solvated and partially desolvated samples, verified the existence of Fe(II) state in 1·2DMF·H_2O, and the existence of a high-spin to low-spin transition in the Fe(II) centers of the partially desolvated sample 1·2DMF. Interestingly, 1·2DMF also exhibits photo-induced SCO phenomenon at low temperature with T_{LIESST} of 60 K. Reversible ON/OFF photo-switching of 1·2DMF was possible through consecutive exposure to 532 and 808 nm laser light, validating the reversible photo-conversion of the metastable $(Mo^{V}_{LS})(Fe^{II}_{HS})_2$ state to the ground $(Mo^{V}_{LS})(Fe^{II}_{LS})_2$ state at 10 K. The gas adsorption study on 1·2DMF confirms the porous nature of the sample. The present research work towards the synthesis of new ambient temperature bistable materials with the LIESST effect opens a new pathway towards the development of moisture sensing and optically active multifunctional materials.

Experimental

All chemicals were used as purchased from chemical sources without further purification. The building block $[HNBu_3]_3[Mo(CN)_8]$ was prepared by the literature procedures.[37, 38]

Synthesis of $\{[Mo^{V}(CN)_8][Fe^{II}(v\text{-}im)_4]_2\cdot BF_4\}_n\cdot 2DMF\cdot H_2O$ (1·2DMF·H_2O)

The reaction of $[HBu_3N]_3[Mo^{V}(CN)_8]$ (43.2 mg, 0.05 mmol) with $Fe(BF_4)_2.6H_2O$ (16 mg, 0.05 mmol) in DMF (2 mL) produces a light yellow solution. A solution of Vinyl-imidazole (42.3, 0.45 mmol) in DMF (1 mL) was added dropwise. The resulting green solution was stirred for 10 min and filtered off. Greenish yellow block shape crystals of 1·2DMF·H_2O were obtained in 60 % yield from long standing of the filtrate. For 1·2DMF·H_2O: $C_{54}H_{64}BF_4Fe_2MoN_{26}O_3$ (M.W. 1419.73 g mol^{-1}) Anal. Calcd.: C, 45.68; H, 4.54; N, 25.65. Found: C, 45.71; H, 4.57; N, 25.68. IR (ATR, cm^{-1}): 3506, 3120, 3032, 2963, 2938, 2876, 2167, 2142, 1655, 1523, 1509, 1470, 1382, 1331, 1285, 1233, 1095, 1009, 930, 897, 841, 761, 694, 666, 602 and 594. For 1·2DMF: $C_{54}H_{62}BF_4Fe_2MoN_{26}O_2$ (M.W. 1401.71 g mol^{-1}) Anal. Calcd.: C, 46.27; H, 4.46; N, 25.98. Found: C, 46.01; H, 4.53; N, 26.10.

Physical measurements

The elemental analyses of C, H, and N were performed with Thermo Scientific Flash 2000 Organic Elemental Analyzer. Infrared (IR) spectra were recorded in the range of 4000 – 550 cm^{-1} on PerkinElmer FT-IR Frontier spectrometer. UV-vis-NIR spectra were carried out in the region of 250 – 2000 nm on a Lambda 1050+ UV-vis-NIR spectrometer. Solid-state UV-vis-NIR measurements were carried out by taking 5% sample by weight in KBr. Thermogravimetric analysis (TGA) was done on a Mettler Toledo TGA/SDTA851 analyzer with a heating rate of 10 °C min^{-1} under a nitrogen atmosphere ranging from 30°C to 300 °C. PXRD data analyses were done using PANalytical X'Pert HighScore Plus software.

Magnetic measurements

The magnetic susceptibility measurements were performed with Quantum Design MPMS-XL EverCool SQUID Magnetometer, between 1.9 K and 350 K for dc applied fields ranging from -5 T to + 5 T. Polycrystalline sample of **1**·2DMF·H_2O (16.8 mg) introduced in a polypropylene bag (2.9 × 0.6 × 0.02 cm) were subjected to measurements. The temperature-

dependent data were measured using 10000 Oe dc field. The isothermal magnetization data were acquired at 2, 5 and 6 K. M *vs* H measurements were performed at 100 K to check for the presence of ferromagnetic impurities which were found to be absent. The magnetic data were corrected for the sample holder and the diamagnetic contribution. The *ac* susceptibility measurements were measured with an oscillating *ac* field of 3 Oe with frequency between 1 to 1500 Hz.

(Photo)Magnetic measurements were carried out by using a sample holder inside the Quantum Design MPMS-XL EverCool SQUID magnetometer equipped with an optical fiber. In a typical experiment, 1.5 mg of finely ground crystals were deposited on an adhesive tape. The sample was separated from the end of the optical fiber by 6.5 cm. All the irradiations were carried out at 10 K to minimize the temperature variation induced by the light. The experimental data were corrected for the diamagnetic contribution of the constituent atoms as well as by the residual diamagnetic signal from the holder. Note that the temperatures have been corrected to consider the light irradiation heating. Experimental susceptibilities were corrected for sample holder and intrinsic diamagnetic contribution.

Gas Adsorption Study

To conduct gas adsorption study on complex **4.1**.2DMF, the pretreatment of the sample was done at 343 K under high vacuum (10^{-1} Pa) for 4 hours. The N_2 sorption studies were performed with approx. 50 mg sample using BELSORP MAX II analyzer at 77 K temperature.

Optical measurements

The surface reflectivity measurements have been performed with a home-built system, operating between 10 and 300 K and in a spectrometric range from 365 nm to 1050 nm. A halogen-tungsten light source (Leica CLS 150 XD tungsten halogen source with a fixed power of 0.5 mW/cm^2) was used as the spectroscopic light. The measurements were calibrated by barium sulphate as a reference sample. With this reflectivity technique, the absolute reflectivity (AR) at a specific wavelength λ is plotted as AR (λ = ($R_{sample}(\lambda)$ -$R_{dark}(\lambda)$) / ($R_{ref}(\lambda)$ -$R_{dark}(\lambda)$). The corresponding spectra AR (λ) can be viewed as a mirror image of the absorbance spectra: i.e., when the sample absorbs efficiently (or weakly) the light, a low (or high, respectively) value of AR is measured. Irradiations were done with the spectroscopic white light (0.5 mW/cm^2) and a set-up of 14 different Light Emitting Diodes (high power LEDs from Thorlabs) operating between 365 nm and 1050 nm with an adjustable power (up to 160 mW/cm^2). As the samples are potentially very photo-sensitive, the light exposure time was minimized during the experiments keeping the samples in the dark except during the spectra measurements when white light is shined on the sample surface (Power = 0.5 mW/cm^2). For all the excitation/de-excitation experiments performed at 10 K, the sample was initially placed at 300 K and then at the low temperature keeping the sample in the dark to avoid any excitation. Heating and cooling measurements were carried out at 5 K/min, whereas the relaxation experiment was performed with a sweep rate of 0.5 K/min. For white light irradiation, the source described above was used, but continuously with a power of 0.5 mW/cm^2 and the light is only switched on for 1 second to record the reflectivity spectrum at a given temperature, and then the light is switched off during the next temperature step.

X-ray crystallography

Single–crystal X–ray structure diffraction studies of complex **1**·2DMF·H_2O were performed with a Bruker SMART APEX CCD diffractometer equipped with graphite–monochromated Mo Kα radiation (λ = 0.71073 Å). The single crystal was mounted on a crystal mounting loop with the help of Paratone oil at 296 K and slowly cooled down to the measured temperature 120 K with 2 K/min ramping rate using a liquid nitrogen gas-stream cooling device, followed by data collection at respective temperatures. Data integration and reduction were carried out using SAINT software, and empirical absorption corrections were performed using SADABS program.[39] The structures were solved by direct methods and refined using full-matrix least-squares method on F2 with SHELXL-2014.[40] The packing diagrams were made using Mercury 4.2.0.[41]

The disordered non-hydrogen atoms belonging to the solvent molecules were refined isotropically. Moreover, hydrogen atoms could not be assigned to the solvent molecules, though, considered in the molecular formula. All other non-hydrogen atoms of complex **1**·2DMF·H_2O were refined anisotropically and hydrogen atoms were labeled to ideal positions and refined isotropically using a riding model. Complex **1**·2DMF·H_2O at 120 and 240 K contains severely disordered BF_4^- molecules, which were treated by using SOLVENT MASK procedure in OLEX 2 which is equivalent to SQUEEZE in PLATON. Additional information about the SOLVENT MASK procedure and corresponding results can be found in the cif files.

The Single–crystal X–ray structure diffraction studies of complex **1**·2DMF was performed at the X-ray diffraction beamline (XRD1) of the Elettra Synchrotron (Trieste, Italy).[42] The crystals were dipped in NHV oil (Jena Bioscience, Jena, Germany) and mounted on the goniometer head with nylon loops (MiTeGen, Ithaca, USA). Data were acquired using a monochromatic wavelength of 0.70 Å through the rotating crystal method on a Pilatus 2M hybrid-pixel area detector (DECTRIS Ltd., Baden-Daettwil, Switzerland). The diffraction data were indexed and integrated using XDS.[43] The structure was solved with Olex2[44] by using ShelXT[45] structure solution program by Intrinsic Phasing and refined with the ShelXL[46] refinement package using least-squares minimization. In the last cycles of refinement, non-hydrogen atoms were refined anisotropically. Hydrogen atoms were included in calculated positions, and a riding model was used for their refinement. The crystal **1**·2DMF·H_2O was mounted directly at 350 K using XRD1 beamline at Elettra Sincrotrone to remove the water molecule (confirmed by TGA data) and then we measured the structure at 270 K quickly. The data quality of **1**·2DMF was not great due to the degradation of the crystal at high temperature. However, we were able to see the structure of partially desolvated **1**·2DMF form which has no water molecule present. We have

tried to get the low temperature structures of **1**·2DMF but unable to get reasonable dataset to get the proper crystal structure.

CCDC 23355698, 2335708 and 2336287 contain the supplementary crystallographic data for this paper. These data can be obtained free of charge from The Cambridge Crystallographic Data Centre via www.ccdc.cam.ac.uk/data_request/cif.

Author Contributions

KK: investigation, data curation, formal Analysis, synthetic and experimental methodology, writing – original draft. SP: synthetic methodology. SM: investigation (magnetic measurement), editing. SK: investigation (single crystal XRD). RL and YL: investigation (photomagnetic measurement). PKM: investigation (single crystal XRD). MR: investigation (optical reflectivity). JP: investigation (Mössbauer Studies). AM: conceptualization, supervision, funding acquisition, writing – review and editing.

Conflicts of interest

There are no conflicts to declare.

Acknowledgements

This research work is supported by the Indian Institute of Science (IISc), Bangalore, India; the Department of Science and Technology, Mission on Nano Science and Technology (Nano Mission) (DST, Project No. DST/NM/TUE/QM-10/2019(G)/1), Government of India. We gratefully acknowledge the "Italian Ministry of Foreign Affairs and International Cooperation and the Indian Department of Science & Technology" for the support to access the Elettra synchrotron Beamline. KK, SP, SK, SM thanks to IISc for their fellowship.

Notes and references

1. P. Gütlich, Y. Garcia and H. A. Goodwin, Spin crossover phenomena in Fe() complexes, *Chem. Soc. Rev.*, 2000, **29**, 419-427.
2. Y. Pan, Y.-S. Meng, Q. Liu, W.-Q. Gao, C.-H. Liu, T. Liu and Y.-Y. Zhu, Construction of SCO-Active Fe(II) Mononuclear Complexes from the Thio-pybox Ligand, *Inorg. Chem.*, 2020, **59**, 7398-7407.
3. S.-i. Ohkoshi, K. Imoto, Y. Tsunobuchi, S. Takano and H. Tokoro, Light-induced spin-crossover magnet, *Nat. Chem.*, 2011, **3**, 564-569.
4. X. Li, D. Zhang, Y. Qian, W. Liu, C. Mathonière, R. Clérac and X. Bao, Chemical Manipulation of the Spin-Crossover Dynamics through Judicious Metal-Ion Dilution, *J. Am. Chem. Soc.*, 2023, **145**, 9564-9570.
5. S. Brooker, Spin crossover with thermal hysteresis: practicalities and lessons learnt, *Chem. Soc. Rev.*, 2015, **44**, 2880-2892.
6. J. Villalva, A. Develioglu, N. Montenegro-Pohlhammer, R. Sánchez-de-Armas, A. Gamonal, E. Rial, M. García-Hernández, L. Ruiz-Gonzalez, J. S. Costa, C. J. Calzado, E. M. Pérez and E. Burzurí, Spin-state-dependent electrical conductivity in single-walled carbon nanotubes encapsulating spin-crossover molecules, *Nat. Commun.*, 2021, **12**, 1578.
7. E. Resines-Urien, E. Fernandez-Bartolome, A. Martinez-Martinez, A. Gamonal, L. Piñeiro-López and J. S. Costa, Vapochromic effect in switchable molecular-based spin crossover compounds, *Chem. Soc. Rev.*, 2023, **52**, 705-727.
8. F. J. Valverde-Muñoz, M. Seredyuk, M. Meneses-Sánchez, M. C. Muñoz, C. Bartual-Murgui and J. A. Real, Discrimination between two memory channels by molecular alloying in a doubly bistable spin crossover material, *Chem. Sci.*, 2019, **10**, 3807-3816.
9. J. Dugay, M. Aarts, M. Giménez-Marqués, T. Kozlova, H. W. Zandbergen, E. Coronado and H. S. J. van der Zant, Phase Transitions in Spin-Crossover Thin Films Probed by Graphene Transport Measurements, *Nano Lett.*, 2017, **17**, 186-193.
10. E. Coronado, Molecular magnetism: from chemical design to spin control in molecules, materials and devices, *Nat. Rev. Mater.*, 2020, **5**, 87-104.
11. O. Kahn and C. J. Martinez, Spin-Transition Polymers: From Molecular Materials Toward Memory Devices, *Science*, 1998, **279**, 44-48.
12. M. Oppermann, F. Zinna, J. Lacour and M. Chergui, Chiral control of spin-crossover dynamics in Fe(II) complexes, *Nat. Chem.*, 2022, **14**, 739-745.
13. S. Ghosh, S. Kamilya, T. Pramanik, M. Rouzières, R. Herchel, S. Mehta and A. Mondal, ON/OFF Photoswitching and Thermoinduced Spin Crossover with Cooperative Luminescence in a 2D Iron(II) Coordination Polymer, *Inorg. Chem.*, 2020, **59**, 13009-13013.
14. R. W. Hogue, S. Singh and S. Brooker, Spin crossover in discrete polynuclear iron(ii) complexes, *Chem. Soc. Rev.*, 2018, **47**, 7303-7338.
15. N. Pittala, F. Thétiot, S. Triki, K. Boukheddaden, G. Chastanet and M. Marchivie, Cooperative 1D Triazole-Based Spin Crossover FeII Material With Exceptional Mechanical Resilience, *Chem. Mater*, 2017, **29**, 490-494.
16. K. Kaushik, S. Mehta, M. Das, S. Ghosh, S. Kamilya and A. Mondal, Stimuli-responsive magnetic materials: impact of spin and electronic modulation, *Chem. Commun.*, 2023, **59**, 13107-13124.
17. H. Phan, J. J. Hrudka, D. Igimbayeva, L. M. Lawson Daku and M. Shatruk, A Simple Approach for Predicting the Spin State of Homoleptic Fe(II) Tris-diimine Complexes, *J. Am. Chem. Soc.*, 2017, **139**, 6437-6447.
18. S. Ghosh, S. Bagchi, S. Kamilya and A. Mondal, Effect of ligand substituents and tuning the spin-state switching in manganese(iii) complexes, *Dalton Trans.*, 2021, **50**, 4634-4642.
19. S. Kamilya, S. Mehta, M. Semwal, R. Lescouëzec, Y. Li, J. Pechousek, V. R. Reddy, E. Rivière, M. Rouzières and A. Mondal, ON/OFF Photo(switching) along with Reversible Spin-State Change and Single-Crystal-to-Single-Crystal Transformation in a Mixed-Valence Fe(II)Fe(III) Molecular System, *Inorg. Chem.*, 2023, **62**, 8794-8802.
20. K. Kaushik, S. Ghosh, S. Kamilya, M. Rouzières, S. Mehta and A. Mondal, Reversible Photo- and Thermo-Induced Spin-State Switching in a Heterometallic {5d-3d} W2Fe2 Molecular Square Complex, *Inorg. Chem.*, 2021, **60**, 7545-7552.

21. A. Mondal, Y. Li, L.-M. Chamoreau, M. Seuleiman, L. Rechignat, A. Bousseksou, M.-L. Boillot and R. Lescouëzec, Photo- and thermo-induced spin crossover in a cyanide-bridged {MoV2FeII2} rhombus molecule, *Chem. Commun.*, 2014, **50**, 2893-2895.
22. S. Chorazy, T. Charytanowicz, D. Pinkowicz, J. Wang, K. Nakabayashi, S. Klimke, F. Renz, S.-i. Ohkoshi and B. Sieklucka, Octacyanidorhenate(V) Ion as an Efficient Linker for Hysteretic Two-Step Iron(II) Spin Crossover Switchable by Temperature, Light, and Pressure, *Angew. Chem. Int. Ed.*, 2020, **59**, 15741-15749.
23. L. Zhao, Y.-S. Meng, Q. Liu, O. Sato, Q. Shi, H. Oshio and T. Liu, Switching the magnetic hysteresis of an [Feii–NC–Wv]-based coordination polymer by photoinduced reversible spin crossover, *Nat. Chem.*, 2021, **13**, 698-704.
24. T. Liu, H. Zheng, S. Kang, Y. Shiota, S. Hayami, M. Mito, O. Sato, K. Yoshizawa, S. Kanegawa and C. Duan, A light-induced spin crossover actuated single-chain magnet, *Nat. Commun.*, 2013, **4**, 2826.
25. S.-i. Ohkoshi and H. Tokoro, Photomagnetism in Cyano-Bridged Bimetal Assemblies, *Acc. Chem. Res*, 2012, **45**, 1749-1758.
26. S.-i. Ohkoshi, S. Takano, K. Imoto, M. Yoshikiyo, A. Namai and H. Tokoro, 90-degree optical switching of output second-harmonic light in chiral photomagnet, *Nat. Photon.*, 2014, **8**, 65-71.
27. H.-L. Zhu, Y.-R. Lei, Y.-S. Meng, T. Liu and H. Oshio, A cyanide-bridged FeII–MoV-based coordination polymer showing spin crossover, *Inorg. Chem. Commun.*, 2022, **146**, 110217.
28. S. Kawabata, S. Chorazy, J. J. Zakrzewski, K. Imoto, T. Fujimoto, K. Nakabayashi, J. Stanek, B. Sieklucka and S.-i. Ohkoshi, In Situ Ligand Transformation for Two-Step Spin Crossover in FeII[MIV(CN)8]4– (M = Mo, Nb) Cyanido-Bridged Frameworks, *Inorg. Chem.*, 2019, **58**, 6052-6063.
29. W. Kosaka, H. Tokoro, T. Matsuda, K. Hashimoto and S.-i. Ohkoshi, Extremely Gradual Spin-Crossover Phenomenon in a Cyano-Bridged Fe−Mo Bimetallic Assembly, *J. Phys. Chem. C*, 2009, **113**, 15751-15755.
30. S. Kawabata, K. Nakabayashi, K. Imoto and S.-i. Ohkoshi, Spin crossover phenomenon in a three-dimensional cyanido-bridged FeII–MoIV assembly, *J. Appl. Phys.*, 2021, **129**, 105501.
31. D. Casanova, M. Llunell, P. Alemany and S. Alvarez, The Rich Stereochemistry of Eight-Vertex Polyhedra: A Continuous Shape Measures Study, *Chem. Eur. J*, 2005, **11**, 1479-1494.
32. R.-J. Wei, Q. Huo, J. Tao, R.-B. Huang and L.-S. Zheng, Spin-Crossover FeII4 Squares: Two-Step Complete Spin Transition and Reversible Single-Crystal-to-Single-Crystal Transformation, *Angew. Chem. Int. Ed.*, 2011, **50**, 8940-8943.
33. T. Nakanishi, Y. Hori, H. Sato, S.-Q. Wu, A. Okazawa, N. Kojima, T. Yamamoto, Y. Einaga, S. Hayami, Y. Horie, H. Okajima, A. Sakamoto, Y. Shiota, K. Yoshizawa and O. Sato, Observation of Proton Transfer Coupled Spin Transition and Trapping of Photoinduced Metastable Proton Transfer State in an Fe(II) Complex, *J. Am. Chem. Soc.*, 2019, **141**, 14384-14393.
34. S. Kamilya, S. Ghosh, Y. Li, P. Dechambenoit, M. Rouzières, R. Lescouëzec, S. Mehta and A. Mondal, Two-Step Thermoinduced Metal-to-Metal Electron Transfer and ON/OFF Photoswitching in a Molecular [Fe2Co2] Square Complex, *Inorg. Chem.*, 2020, **59**, 11879-11888.
35. A. Mondal, Y. Li, P. Herson, M. Seuleiman, M.-L. Boillot, E. Rivière, M. Julve, L. Rechignat, A. Bousseksou and R. Lescouëzec, Photomagnetic effect in a cyanide-bridged mixed-valence {FeII2FeIII2} molecular square, *Chem. Commun.*, 2012, **48**, 5653-5655.
36. C. P. Slichter and H. G. Drickamer, Pressure-Induced Electronic Changes in Compounds of Iron, *J. Chem. Phys.*, 1972, **56**, 2142-2160.
37. A. Mondal, L.-M. Chamoreau, Y. Li, Y. Journaux, M. Seuleiman and R. Lescouëzec, W Co Discrete Complex Exhibiting Photo- and Thermo-Induced Magnetisation, *Chem. - Eur. J.*, 2013, **19**, 7682-7685.
38. J. R. Withers, D. Li, J. Triplet, C. Ruschman, S. Parkin, G. Wang, G. T. Yee and S. M. Holmes, Synthesis and characterization of one- and two-dimensional octacyanometalate(V) networks: {[trans-MII(DMF)4][cis-MII(DMF)4]2[MV(CN)8]2}n (MII=Mn, Fe, Ni; MV=Mo, W), *Polyhedron*, 2007, **26**, 2353-2366.
39. G. M. Sheldrick, SADABS Version 2.03, Bruker Analytical X-Ray Systems, Madison, WI, USA, 2000.
40. G. Sheldrick, Crystal structure refinement with SHELXL, *Acta Crystallographica Section C*, 2015, **71**, 3-8.
41. C. F. Macrae, P. R. Edgington, P. McCabe, E. Pidcock, G. P. Shields, R. Taylor, M. Towler and J. van de Streek, Mercury: visualization and analysis of crystal structures, *J. Appl. Crystallogr.*, 2006, **39**, 453-457.
42. A. Lausi, M. Polentarutti, S. Onesti, J. R. Plaisier, E. Busetto, G. Bais, L. Barba, A. Cassetta, G. Campi, D. Lamba, A. Pifferi, S. C. Mande, D. D. Sarma, S. M. Sharma and G. Paolucci, Status of the crystallography beamlines at Elettra, *The European Physical Journal Plus*, 2015, **130**, 43.
43. W. Kabsch, XDS, *Acta Crystallographica Section D*, 2010, **66**, 125-132.
44. O. V. Dolomanov, L. J. Bourhis, R. J. Gildea, J. A. K. Howard and H. Puschmann, OLEX2: a complete structure solution, refinement and analysis program, *J. Appl. Crystallogr.*, 2009, **42**, 339-341.
45. G. M. Sheldrick, SHELXT - integrated space-group and crystal-structure determination, *Acta crystallographica. Section A, Foundations and advances*, 2015, **71**, 3-8.
46. G. M. Sheldrick, Crystal structure refinement with SHELXL, *Acta crystallographica. Section C, Structural chemistry*, 2015, **71**, 3-8.